

Combined Effect of Carbon Dioxide, Hydrogen Sulfide, and Acetic Acid on Bottom-of-the-Line Corrosion

M. Singer,^{†*} B. Brown,^{*} A. Camacho,^{**} and S. Nešić^{*}

ABSTRACT

This research work presents a study of the combined influence of the partial pressure of hydrogen sulfide (H_2S) and the concentration of free acetic acid (CH_3COOH) on the general and localized carbon dioxide (CO_2) corrosion at the bottom of the line. Experiments were carried out for up to 21 days in three 4-in (101.6-mm) internal diameter flow loops at 70°C with 2 bars of CO_2 . The flow regime was stratified for all of the experiments. It was found that trace amounts of H_2S (from 0.004 bar to 0.13 bar) greatly retards the CO_2 corrosion with general corrosion rates usually 10 to 100 times lower than their pure CO_2 equivalent. However, the most protective conditions were observed at the lowest partial pressure of H_2S , while corrosion increased when more H_2S was added. The presence of a mackinawite film on the coupon surface seems to be the origin of this protectiveness. When 1,000 ppm of free acetic acid was added to the system, the general corrosion rate doubled compared with a baseline CO_2 environment and by between one and two orders of magnitude compared to baseline H_2S/CO_2 mixtures.

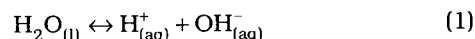
KEY WORDS: acetic acid, bottom-of-the-line corrosion, CO_2 / H_2S corrosion, mackinawite

INTRODUCTION

Carbon dioxide (CO_2) corrosion in the presence of acetic acid (CH_3COOH) has been studied extensively by many different investigators.¹⁻⁶ Consequently, the corrosion mechanisms for this system are now well defined and have been incorporated in prediction models.⁷⁻⁸ The influence of acetic acid on the siderite ($FeCO_3$) film characteristics and formation is one of the last areas where a widely accepted theory is not agreed upon completely.⁹⁻¹² The objective of this paper was to try to improve our understanding of the influence of the partial pressure of hydrogen sulfide (H_2S) and the presence of acetic acid on the CO_2 -influenced corrosion rate of carbon steel and the characteristics of the corrosion product film formed.

The different chemical and electrochemical reactions involved in CO_2 corrosion in the presence of acetic acid are described below:

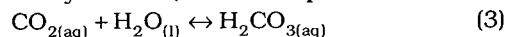
Water dissociation:



Carbon dioxide dissolution:



Carbon dioxide hydration (slowest step):



Carbonic acid dissolution:



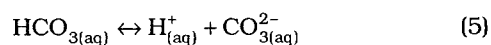
Submitted for publication July 14, 2009; in revised form, July 7, 2010.

[†] Corresponding author. E-mail: singer@ohio.edu.

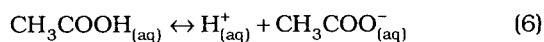
^{*} Ohio University, Institute for Corrosion and Multiphase Technology, 342 West State St., Athens, OH 45701.

^{**} Ohio University, Institute for Corrosion and Multiphase Technology, 342 West State St., Athens, OH 45701. Present address: Lloyd's Register Capstone, Inc., 1505 Hwy. 6 South, Suite 250, Houston, TX 77077.

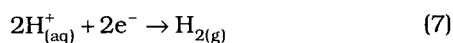
Bicarbonate ion dissociation:



Acetic acid (HAc) dissociation:



Proton reduction:



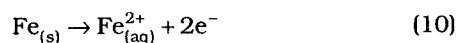
Carbonic acid reduction:



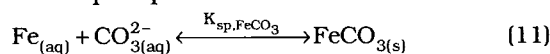
Undissociated acetic acid reduction:



Iron oxidation:



Iron carbonate precipitation:



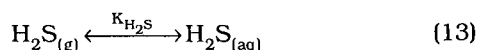
The choice of the expression of the equilibrium constant governing the iron carbonate precipitation/dissolution is also of importance because many empirical equations exist. Recent work proposed by Sun¹³ suggests using the following equation derived from the work of Greenberg and Tomson¹⁴ and Silva, et al.:¹⁵

$$\log K_{\text{sp,FeCO}_3} = -59.3498 - 0.041377 \times T_k - \frac{2.1963}{T_k} + 24.5724 \times \log(T_k) + 2.518 \times I^{0.5} - 0.657 \times I \quad (12)$$

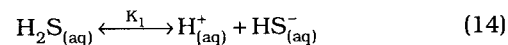
where $K_{\text{sp,FeCO}_3}$ is the solubility constant for iron carbonate (mol^2/L^2), T_k is temperature (K), and I is ionic strength (mol/L).

In addition, as more and more field conditions involve the presence of large quantities of H_2S , the prediction of sour corrosion appears today as one of the most pressing matters in the oil and gas industry.¹⁶ The understanding of H_2S corrosion mechanisms lags clearly behind, even if a lot of effort has already been made in this direction.¹⁷ Although H_2S gas is about three times more soluble than CO_2 gas, the acid created by dissociation of H_2S is about three times weaker than carbonic acid (H_2CO_3). Hence, the effect of H_2S gas on decreasing the solution pH is approximately the same as for CO_2 gas. The different chemical and electrochemical reactions involved in the H_2S corrosion are described below and are added to the list above:

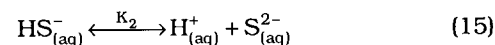
Hydrogen sulfide dissolution:



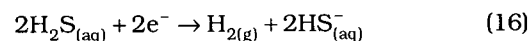
Hydrogen sulfide dissociation:



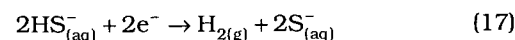
Bisulfide dissociation:



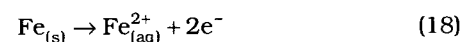
Hydrogen sulfide reduction:



Bisulfide reduction:

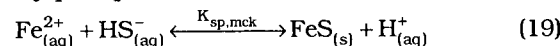


Iron oxidation:

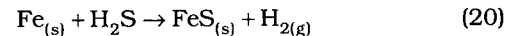


Iron sulfide formation:

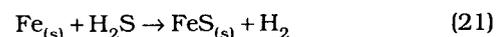
by precipitation:



by direct (solid-state) reaction:



The chemical reactions proposed above are the most widely accepted¹³ reactions describing sulfide chemistry in aqueous solution. Other authors¹⁸⁻²⁰ have proposed different pathways for iron sulfide (FeS) formation and dissolution. An example is the so-called "direct" reaction:



It is assumed that the iron dissolution does not occur, but rather a fast oxidation of solid iron transforms it directly into solid iron sulfide attached to the steel surface. The mechanism of this reaction is still under investigation, including the role of various species in the formation of the different types of iron sulfide.

The uncertainty related to the expressions for the equilibrium constants involved in H_2S aqueous chemistry is much more acute than with CO_2 aqueous chemistry and it is therefore necessary to state precisely what has been used in this work. Sun¹³ postulated the following equations were the most reliable:

from Suleimenov and Krupp:²¹

$$K_{\text{H}_2\text{S}} = 10^{-\left(634.27 + 0.2709T_k - 0.11132 \times 10^{-3}T_k^2 - \frac{16.719}{T_k} - 261.9 \log T_k\right)} \quad (22)$$

from Suleimenov and Seward:²²

$$K_1 = 10^{\frac{782.43 + 0.361T_k - 1.6722 \times 10^{-4}T_k^2 - \frac{20,565.7315}{T_k} - 142.741 \ln T_k}{}} \quad (23)$$

from Benning, et al.:²³

$$K_{\text{sp,mck}} = 10^{\frac{2,848.779}{T_k} - 6.347 + \log(K_1)} \quad (24)$$

where K_{H_2S} is the solubility constant of hydrogen sulfide (mol/L/bar), K_1 is the dissociation constant of H_2S (mol/L), $K_{sp,mck}$ is the solubility limit of mackinawite (FeS) (mol/L), and T_x is temperature (K).

Sun¹³ also stated that there was not yet a reliable expression for the second dissociation constant, K_2 , and the use of this constant to calculate the solubility limit should be avoided altogether. Consequently, to avoid the HS^- dissociation equilibrium constant, the FeS solubility is calculated in the present paper using the following equation:

$$K_{sp,mck} = \frac{[Fe^{2+}] \times [HS^-]}{[H^+]} \quad (25)$$

Some valuable experimental work has been conducted recently to determine the effect of small amounts of H_2S on the CO_2 corrosion of carbon steel.²⁴⁻²⁷ It was shown that small amounts of H_2S lead to a rapid and significant reduction of the CO_2 corrosion rate. The reduction of the corrosion rate is usually associated with the formation of a corrosion product film on the metal surface, even if the bulk conditions for supersaturation of $FeCO_3$ or FeS are not met. The analysis of the film usually shows the presence of a very thin mackinawite film. It has been reported that the formation of mackinawite on mild steel is a very fast, direct surface reaction leading to a solid adherent mackinawite layer.^{18-20,27-28} Depending on various environmental factors, different thermodynamically stable types of FeS can be formed. In some cases FeS film can be nonprotective and result in localized attack. For example, the formed layer can develop internal stresses that can lead to film fracture, causing a potential localized attack problem. Generally, three regimes in CO_2/H_2S systems have been classified based on the concentration of H_2S as shown in Figure 1.²⁹ Nevertheless, the mixed CO_2/H_2S zone has been reported to begin at a much smaller ratio than the one that is displayed in the graph in Figure 1.²⁶ The chemistry of iron sulfide film formation is very complex and the film characteristics and morphology can change with test conditions and time, which can lead to very different corrosivity scenarios. Smith and Pacheco³⁰ reported that there are three main forms of iron sulfide that are commonly found in the field, which are mackinawite, pyrrhotite, and pyrite.

- Mackinawite is a metastable form of FeS that forms in the presence of small amounts of H_2S .
- Pyrrhotite is believed to be more thermodynamically stable than mackinawite because the pyrrhotite formation kinetics are much slower than those of mackinawite.
- The formation of pyrite is associated with high H_2S partial pressure and is believed to require elemental sulfur.

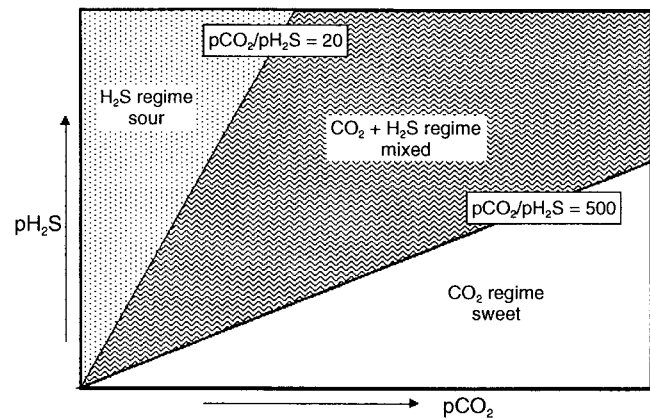


FIGURE 1. Corrosion regimes in CO_2/H_2S corrosion as defined by Pots, et al.²⁹

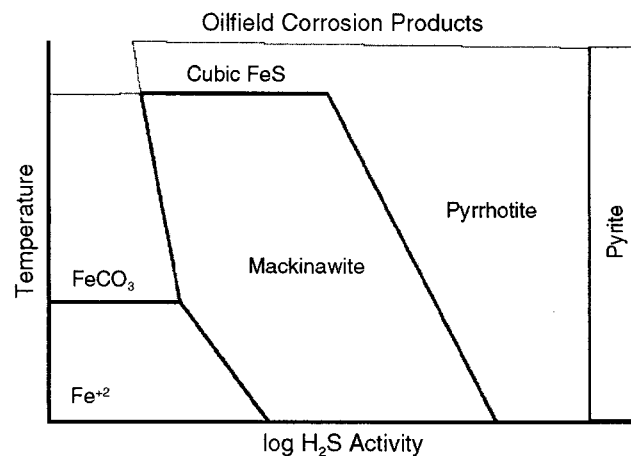


FIGURE 2. Corrosion product formation as a function of temperature and H_2S .³⁰

The corrosion product map related to the formation of these three types of FeS film is shown in Figure 2.

The influence of organic acids on the relative protectiveness of iron sulfide films adds another unknown to the problem since there is, to our knowledge, only one published paper on that subject.³¹

The objective of this paper was to try to improve our understanding of the influence of the partial pressure of H_2S and the presence of acetic acid on the CO_2 -influenced corrosion rate of carbon steel and the characteristics of the corrosion product film formed.

EXPERIMENTAL PROCEDURES

Test Matrix

Table 1 presents the experimental conditions of each test. Only two parameters (free acetic acid concentration and H_2S partial pressure) are varied around a set of baseline conditions (Test 1). The influence of these two parameters are studied separately

TABLE 1
Experimental Conditions

Duration	Acetic Acid Series						H ₂ S Series						Acetic Acid/H ₂ S Series					
	Test 1		Test 2		Test 3		Test 4		Test 5		Test 6		Test 7		Test 8		Test 9	
	Fe ²⁺ pH (ppm)	Fe ²⁺ pH (ppm)	Fe ²⁺ pH (ppm)	Fe ²⁺ pH (ppm)	Fe ²⁺ pH (ppm)													
At start	NA ^(A)	NA	3.4	NA	NA	NA	4.2	7.9	4.3	9	4.4	6.5	4.8	40	4.4	56.3	3.9	76
After 2 days	4.6	0.4	NA	NA	3.9	70	4.4	19	4.4	NA	4	25	NA	NA	4.2	145	4.3	94
After 7 days	4.9	8.4	NA	10	3.6	40	4.4	19	4.5	NA	4.1	23	4.7	NA	4.5	110	4.3	NA
After 14 days	4.6	11	4	24	3.7	36	4.6	NA	4.4	18	4.3	25	4.7	70	4.5	150	4.1	170
After 21 days	4.8	11	4	17	3.7	32	4.7	18	4.5	20	4.3	26	4.7	35	4.6	170	4.3	140

^(A) Not available.

TABLE 2
Saturation Level with Regard to FeCO₃ and FeS

Test No.	Test 1	Test 2	Test 3	Test 4	Test 5	Test 6	Test 7	Test 8	Test 9
FeCO ₃ saturation ^(A)	0.12	0.005	0.002	0.13	0.06	0.03	0.24	0.7	0.13
FeS saturation ^(A)	0	0	0	1.6	12	11	3	9	62

^(A) Calculations are made using solubility constants obtained by Sun.¹³

TABLE 3
Acetic Acid Concentration

Test No.	Measured Total Acetate Species ([free HAc] + [Ac ⁻]) in the Liquid Phase with Ion Chromatograph (ppm)	Calculated Free Acetic Acid Concentration in the Liquid Phase (ppm)	
		Based on the Amount of Acetate Species Measured with Ion Chromatography	Based on the Amount of Acetate Species Introduced in the Experimental Loop
Test 2	57	Between 50 and 55	Between 87 and 96
Test 3	675	Between 605 and 664	Between 895 and 944
Test 7	NA	NA	Between 46 and 57
Test 8	1,052	Between 656 and 846	Between 630 and 810
Test 9	1,120	Between 861 and 1,002	Between 772 and 895

(Tests 2 through 6) and then combined in Tests 7, 8, and 9. A set of measurements performed throughout the tests (pH measurement, iron, and acetic acid concentrations) is presented in Tables 2 and 3.

The nine experiments conducted can be divided into three groups investigating different aspects of the corrosion process in a CO₂ environment:

- influence of the concentration of free acetic acid
- influence of the partial pressure of H₂S
- combined effect of the concentration of free acetic acid and the partial pressure of H₂S

Apart from the acetic acid concentration and the partial pressure of H₂S, all the other experimental parameters were kept at a fixed value (system temperature: 70°C, partial pressure of CO₂: 2 bars, total pressure: 3 bars, gas velocity: 5 m/s). The sweet and sour tests were performed in two similar but independent flow loops. The design of the "sour" loop requires

higher liquid flow rate for lubrication purposes. The values of liquid flow rates were, consequently, slightly different between the sour and sweet tests. The primary concern was to ensure that the flow regime was stratified with a superficial liquid velocity determined to be below 0.05 m/s.

EXPERIMENTAL LOOP

Three different large-scale flow loops were used in this study. Experiments were carried out in multiphase, stratified flow with water and a mixture of CO₂/N₂/H₂S. The flow loops, made of Type 316 (UNS S31600)⁽¹⁾ stainless steel and Alloy C276 (UNS N10276) (for the H₂S experiments) all have very similar characteristics and can be divided in three main component parts: the tank, the pump, and the loop.

—The tank (2,000 L) is used for the liquid phase conditioning and heating. It is filled with deionized water. Acetic acid is added to reach the requirements of the tests. A set of immersion heaters control the temperature.

⁽¹⁾ UNS numbers are listed in *Metals and Alloys in the Unified Numbering System*, published by the Society of Automotive Engineers (SAE International) and sponsored by ASTM International.

- Positive displacement progressive cavity pumps or a gas blower are used to move the liquid or the gas phase.
- The 4-in (101.6-mm) diameter flow loop is 30 m long and horizontally leveled. The test sections, where the measurements are taken, are located at least 8 m downstream from the exit of the tank. The test sections (Figure 3) are 1.5-m-long pipe spool pieces. Each has up to four probe ports (two at the top, two at the bottom). In this paper, only the bottom-of-the-line results are taken into account. Samples of condensed liquid and in situ pH measurements were taken at the test section.

More complete presentations of these loops have been published previously in the open literature,^{26,32-33} and the reader is directed to consult these publications for more detailed information.

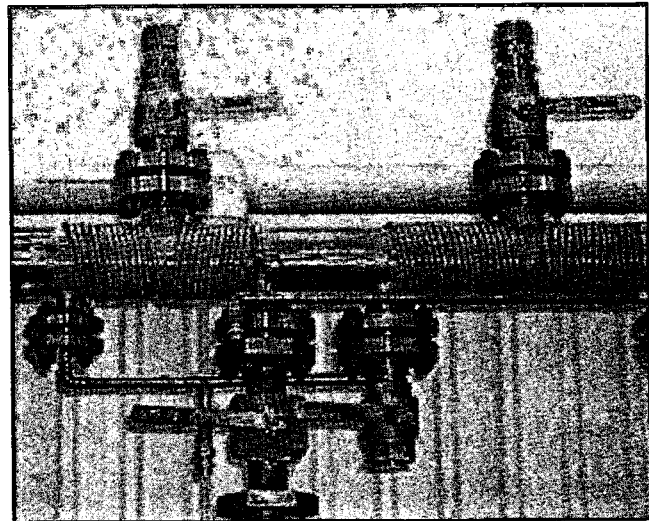


FIGURE 3. Test section of the H_2S loop. Only the bottom ports were used in this study.

EXPERIMENTAL PROCEDURES

The tank was filled first with 1 m³ of deionized water. Carbon dioxide (and nitrogen in some cases) was injected in the loop at a specific pressure. The liquid phase then was heated up to the specific temperature by two electrical resistance heaters. The pump was started and the gas/liquid mixture flowed around the loop in a stratified flow regime. Deoxygenation was performed by depressurizing several times until the concentration of oxygen had been reduced sufficiently (<50 ppb) so as to not affect the overall corrosion process.³⁴ Oxygen concentration was measured using colorimetric test kits. Once the deoxygenation was completed, acetic acid and/or H_2S concentrations were adjusted (see procedures below) to the required levels. The corrosion probes then were introduced under pressure at the test section, which was equipped with two probe ports and the experiment began. Typically, two weight-loss coupons were introduced at the beginning of the test and replaced after 2 days of exposure. Then, 7 days later, one coupon was replaced once again and the experiment continued for an additional 14 days. This way, there were indications of the corrosion rate after 2, 7, 14, and 21 days of testing. A data-acquisition device was used to measure the total pressure and the gas/liquid temperature continuously.

Liquid Phase Specification

The liquid phase was made up exclusively from deionized water. No salt was added. However, dissolved ferrous iron (Fe^{2+}) buildup occurred throughout the test as a result of the corrosion process on the weight-loss coupons. Samples were taken regularly from the liquid phase; Table 2 presents the evolution of Fe^{2+} concentration (obtained using a spectrophotometer) and pH during the whole duration of the tests.

TABLE 4
Chemical Analysis of the Carbon Steels
Used in the Experiments

Element	X65 Composition (%)	API 5L X65 (%)
C	0.13	<0.26
Mn	1.16	<1.40
P	0.009	<0.03
S	0.009	<0.03

Scale Formation

The pH of the liquid phase at the bottom of the line was kept at a value around 4 to 4.5 in each test and the solution was always undersaturated with regard to iron carbonate precipitation. Therefore, $FeCO_3$ was not expected to form on the metal surface in any of the tests performed. On the other hand, the solution was always supersaturated with regard to FeS (in the tests with H_2S). The saturation levels for each type of scale are displayed in Table 4 with supersaturation achieved when values were more than 1.

Acetic Acid Concentration

The acetic acid (HAc) concentration was adjusted by adding a calculated amount of pure HAc in the tank. The acetic acid solution was deoxygenated first before being introduced into the tank using a high-pressure vessel connected to the tank. Several liquid samples then were taken and analyzed by ion chromatography to verify the concentration of the total acetate species (free HAc + Ac^-) present in the liquid phase. The concentration distribution of free HAc and acetate (Ac^-) was calculated from the measured value of pH. A differentiation was made between the free or undissociated acetic acid concentration (free HAc) and the total acetic acid concentration, which included

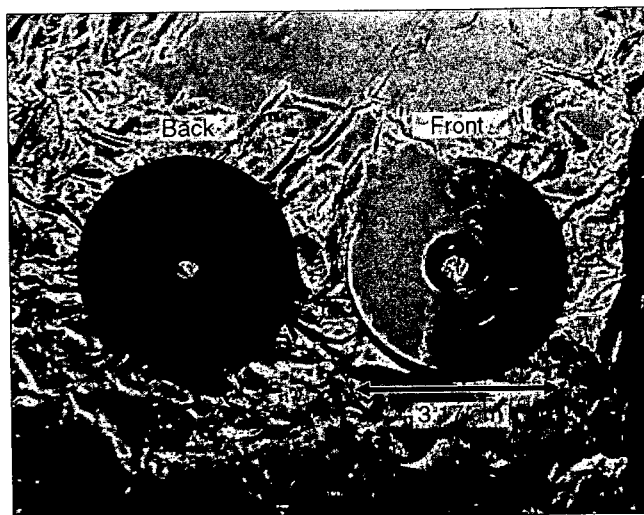


FIGURE 4. Weight-loss coupons with PTFE coating at the back and the side (external diameter = 3.17 cm).

all acetate-containing species (free HAc and acetate Ac^-). To keep the concentration of free acetic acid constant during the test, the pH of the liquid phase was adjusted if necessary by adding more acetic acid.

Table 3 presents the calculated free acetic concentration at the bottom of the line for each test. Ion chromatograph measurements providing total acetate species concentration ($[\text{HAc}]_{\text{free}} + [\text{Ac}^-]$) are shown where available. A range of concentration is provided each time to take into account the change in pH. The calculations of free undissociated acetic acid concentration were performed using the equilibrium constant of acetic acid dissociation proposed by Kharaka, et al.,³⁵ and the following equation (the total acetate species concentration ($[\text{HAc}]_{\text{free}} + [\text{Ac}^-]$) is known:

$$[\text{HAc}]_{\text{free}} = \frac{([\text{HAc}]_{\text{free}} + [\text{Ac}^-]) \times [\text{H}^+]}{K_{\text{HAc}} + [\text{H}^+]} \quad (26)$$

It is important to note that the calculated concentration of free acetic acid was close to the required concentration, but there was, in most cases, a 20% to 30% discrepancy. This discrepancy is most likely from the technical difficulties often met in large-scale loop tests to keep a high degree of accuracy in the measurements but also includes errors in the measurement process. For clarity purposes, the concentration of free acetic acid will be displayed as 100 ppm or 1,000 ppm (depending on the test conditions) throughout this paper.

Gas Phase Composition

In all the experiments, the gas phase was made of a mixture of CO_2 and N_2 (2 bars of CO_2 and 0.7 bars of N_2 , 0.3 bars of water vapor) for a total pressure of 3 bars. For the H_2S environment, the required amount

of H_2S was introduced in pure gas form at the beginning of the test and checked regularly using a piston pump and low-range standard detection tubes. The length of color change in the detection tube reagent was measured using calipers to increase the accuracy of the value. Repeatability of this method was found to be $\pm 5\%$. The trace amounts of H_2S introduced in the loop were consumed fairly rapidly by the corrosion process and the H_2S partial pressure had to be adjusted almost every day to be kept within 20% of the targeted value.

Corrosion Rate Measurement

The weight-loss coupons were not inserted into the corrosion environment until the system had reached steady state (stable temperature, pressure, and flow velocities). The corrosion rates were measured with weight-loss coupons made of API X65 carbon steel. Samples consisting of circular coupons (0.76 cm internal diameter, 3.17 cm external diameter, 0.5 cm thickness) with an exposed area of 7.44 cm^2 were polished using isopropanol ($\text{C}_3\text{H}_8\text{O}$) as coolant on silicon carbide (SiC) papers, up to 600 grit. After this preparation, they were covered with liquid polytetrafluoroethylene (PTFE) on the outer edges and underside (Figure 4). Following 4 h to 6 h of curing at ambient conditions, the samples were held at 200°C in an oven for 30 min according to manufacturer's recommendations. The uncovered steel surface was then repolished with 600-grit SiC paper wetted with isopropanol, cleaned, dried, and weighed. A picture of a coupon after preparation is shown in Figure 4. The coupons then were flush-mounted on the internal pipe wall of the loop by using a specially designed probe holder. Therefore, only one face of the coupon was in direct contact with the corrosive environment. The exposure time was between 2 days and 21 days in all experiments. Upon removal from the loop, the coupon surface was flushed with isopropanol, to dehydrate it, and images of the surface were taken. The weight of the coupon after each test was registered. The ASTM G1³⁶ standard procedure was followed to remove the corrosion products and determine the corrosion rate by weight loss. One coupon is generally used for weight loss, and the other is preserved for corrosion product evaluation by scanning electron microscopy (SEM) and energy-dispersive x-ray spectroscopy (EDS).

Materials Characterization

Weight-loss coupons were machined from API X65 carbon steel prepared from the same piece of field pipe line (33-cm outside diameter pipe section, 3.8 in [96.52 mm] thickness). The chemical analyses of this X65 steel is shown in Table 5. Figure 5 shows the microstructure of longitudinal and transversal cuts of the X65 carbon steel. In this case, only the face of the coupon that would be in contact with the fluid was

TABLE 5
Hardness (HRB) Results

	X65 Longitudinal Cut	X65 Transversal Cut
1	81.3	60.3
2	94.4	68.7
3	98.7	63.3
4	87.9	78.0
5	95.4	59.1
6	89.3	51.1
7	88.7	66.5
8	92.9	75.0
9	93.3	58.5
10	85.1	67.7
Average	90.7	64.8
Approx. tensile strength	90,000 psi for 90.7 HRB	56,000 psi for 65.7 HRB
Tensile requirements	77,000 psi (min.)	77,000 psi (min.)
Yield strength	65,000 psi (min.)	65,000 psi (min.)

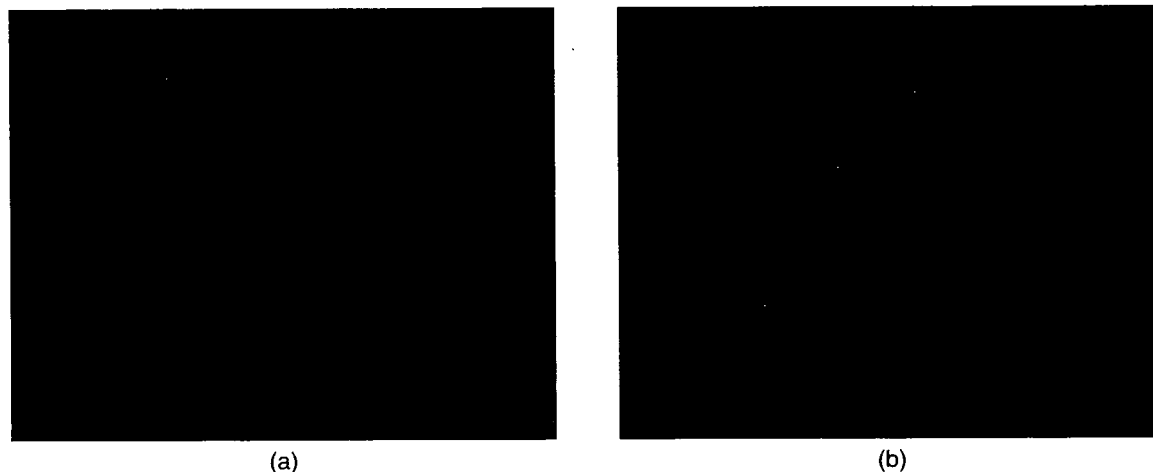


FIGURE 5. Microstructure of the X65 carbon steel: (a) longitudinal cut and (b) transversal cut.

TABLE 6
Test Matrix

Investigating Experiment No.	Acetic Acid			H ₂ S			Acetic Acid/H ₂ S		
	1	2	3	4	5	6	7	8	9
Free HAc tank (ppm)	0	100	1,000	0	0	0	100	1,000	1,000
pH ₂ S (bar)	0	0	0	0.004	0.07	0.13	0.004	0.004	0.13

Common parameters—steel type: API X65; liquid phase composition: DI water; test duration: 3 weeks; absolute pressure: 3 bars; pCO₂: 2 bars; gas temperature: 70°C; gas velocity: 5 m/s; superficial liquid velocity: <0.05 m/s.

evaluated. Cuts were made using cooling fluids and the proper metallographic diamond blade to avoid modifications of the microstructure. The microstructure of the X65 was finer in the longitudinal direction, probably as a result of processing. Figure 5 shows a microstructure typical of a microalloyed thermomechanical controlled processing (TMCP) pipeline steel. Iron carbide was distributed in spheroidized form instead of a lamellar arrangement. Hardness measurements are recorded in Table 6. By converting these values,³⁷ approximate tensile strength was cal-

culated and compared with the values designated for the metal in the standards. The X65 showed a difference in hardness with direction. This change in hardness is consistent with the change in microstructure previously described.

RESULTS AND DISCUSSION

Corrosion Rate Results

Corrosion rate results are displayed in a series of graphs, Figures 6 through 12. Error bars representing

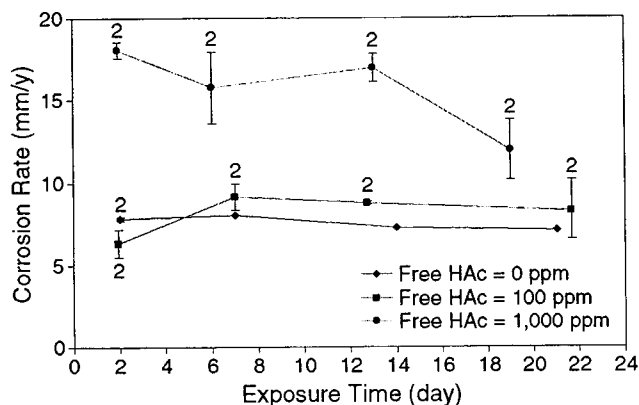


FIGURE 6. Influence of the free HAc concentration. Evolution of the general corrosion rate over time. (Absolute pressure $[P_T]$: 3 bars, partial pressure of CO_2 $[p\text{CO}_2]$: 2 bars, pH_2S : 0 bar, gas temperature $[T_g]$: 70°C , gas velocity $[V_g]$: 5 m/s, superficial liquid velocity $[V]$: < 0.05 m/s).

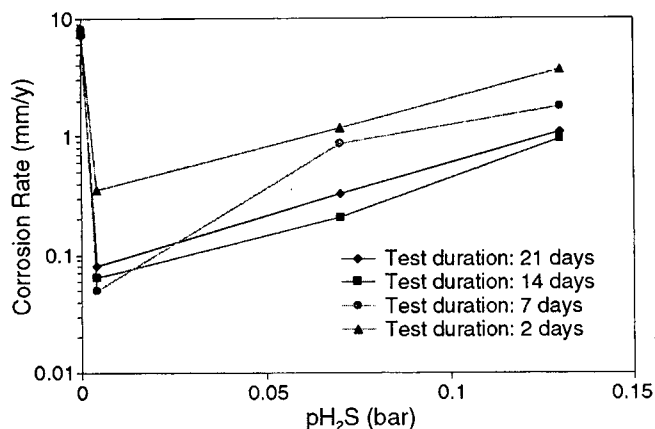


FIGURE 8. Influence of the partial pressure of H_2S . Evolution of the general corrosion rate over time. (P_T : 3 bars, $p\text{CO}_2$: 2 bars, HAc: 0 ppm, T_g : 70°C , V_g : 5 m/s, V_l : < 0.05 m/s).

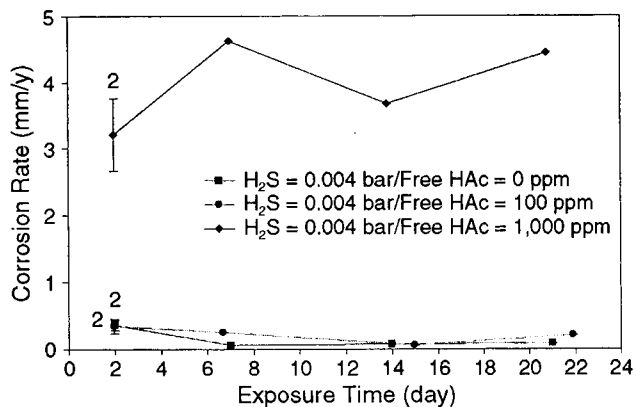


FIGURE 9. Combination of the partial pressure of H_2S and the concentration of free HAc. Evolution of the general corrosion rate over time. (P_T : 3 bars, $p\text{CO}_2$: 2 bars, pH_2S : 0.004 bar, T_g : 70°C , V_g : 5 m/s, V_l : < 0.05 m/s).

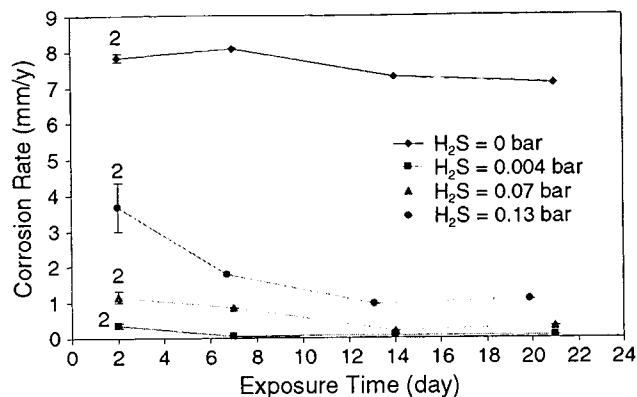


FIGURE 7. Influence of partial pressure of H_2S . Evolution of the general corrosion rate with partial pressure of H_2S . (P_T : 3 bars, $p\text{CO}_2$: 2 bars, free HAc: 0 ppm, T_g : 70°C , V_g : 5 m/s, V_l : < 0.05 m/s).

maximum and minimum values and the number of coupons (number of repeated measurements) are displayed when applicable on each graph.

Influence of the Free Acetic Acid Concentration

The observed influence of the free acetic acid concentration on the average corrosion rate was not surprising. The acetic acid acted as a provider of protons and at the same time added a new cathodic reaction via the direct reduction of undissociated acetic acid. Therefore, in the absence of protective corrosion product film (as is the case here), the average corrosion rate increased when free acetic was present. As is shown in Figure 6, the corrosion rate doubled if 1,000 ppm of free acetic acid was introduced in solution, reaching a maximum well above 10 mm/y. In all cases, the corrosion rate might have varied slightly with time but was expected to remain rather high, since no protective film could form in the severe conditions tested (pH always below 4.5).

Influence of the Partial Pressure of Hydrogen Sulfide

Results related to the influence of the partial pressure of H_2S are shown in Figures 7 and 8, which represent the same data but are displayed in different ways for purposes of clarity. The first H_2S partial pressure tested was 0.004 bar at a $\text{CO}_2/\text{H}_2\text{S}$ ratio of 500 (at the limit between the reported sweet and mixed regimes). However, there was obviously an overwhelming effect of H_2S since the corrosion rates were globally reduced to 0.08 mm/y (almost a factor of 100). As more H_2S was added up to 0.07 bar and 0.13 bar (corresponding to $\text{CO}_2/\text{H}_2\text{S}$ ratio of, respectively, 29 and 15), the tendency was reversed with the average corrosion rate being only 10 to 20 times lower as compared to the pure CO_2 environment. With 0.13 bar of H_2S , the corrosion regime was assumed to be clearly in the so-called "sour regime," i.e., dominated by the presence of H_2S . It is assumed here that the main effect of high H_2S content is the significant rate of the additional cathodic reaction (H_2S reduction) and that

the FeS film formed during these tests has similar protectiveness as in the previous tests with lower partial pressure of H₂S. Moreover, there seemed to be a slight decreasing trend in time in the average corrosion in the presence of H₂S, which could correspond to the gradual formation of a corrosion product film layer. Some FeS films (especially mackinawite) are believed to form almost immediately with small quantities of H₂S and to create a diffusion barrier, which prevents corrosive species (H⁺, H₂CO₃) from reaching the surface.³⁰

Combined Effect of the Acetic Acid and Hydrogen Sulfide — Results are shown in a series of graphs, Figures 9 through 12. While the presence of 100 ppm of acetic acid had little influence on the corrosion rate, the effect was much stronger with 1,000 ppm of free acetic. The influence of this concentration of free acetic acid on the general corrosion rate was even greater compared to the pure CO₂ environment, as described above. The 1,000 ppm of HAC increased the average uniform corrosion rate by 50 times at 0.004 bar H₂S (Figure 9) and 8 times at 0.13 bar H₂S (Figure 10) with an average corrosion rate after 21 days of exposure reaching 4 mm/y and 8 mm/y, respectively. The beneficial effect of the protective sulfide scale shown above was all but completely canceled by the presence of HAC, and the magnitude of the uniform corrosion rate was not acceptable anymore (Figure 11). In the presence of 1,000 ppm of free acetic acid, the partial pressure of H₂S did not seem to have a very strong influence with a corrosion rate being globally half its 'sweet conditions' equivalent (Figure 12).

Surface Analysis

The corrosion product layer was studied systematically for each test using SEM and EDS. However, the complete characterization of corrosion product films (and especially sulfide films) requires x-ray diffraction (XRD) analysis, which, unfortunately, was not performed in this study because of limited availability of the equipment and time constraint. Therefore, even if the visual observations obtained by SEM give some useful indications about the nature of the corrosion product film, some caution should be taken when interpreting the findings.

Influence of the Free Acetic Acid Concentration

— Figure 13 presents typical pictures of the corrosion product film that forms on the surface in a sweet environment when the conditions for FeCO₃ precipitation are not met (low pH). The scale appeared to be uniform and smooth when the coupon was removed from the test loop, but cracks appeared rapidly during the drying process (when isopropanol was sprayed on the coupon surface immediately after the test to dehydrate the steel surface). EDS and SEM analyses of the film were consistent with the notion of cementite (Fe₃C) being the undissolved component of the steel left behind by the corrosion process, although

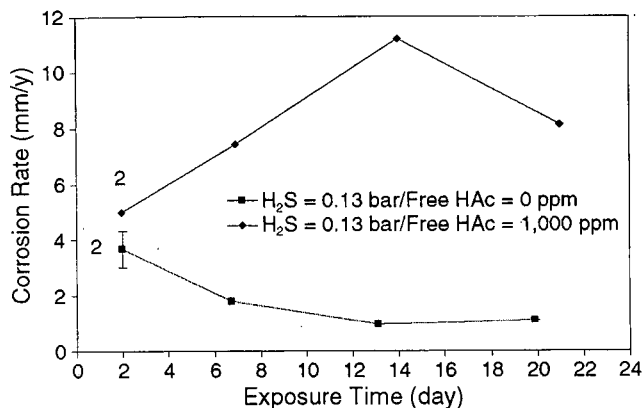


FIGURE 10. Combination of the partial pressure of H₂S and the concentration of free HAC. Evolution of the general corrosion rate over time. (P_T : 3 bars, p_{CO_2} : 2 bars, p_{H_2S} : 0.13 bar, T_g : 70°C, V_g : 5 m/s, V_l < 0.05 m/s).

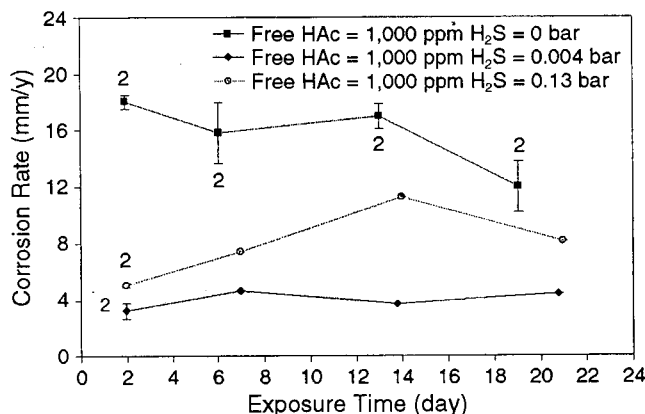


FIGURE 11. Combination of the partial pressure of H₂S and the concentration of free HAC. Evolution of the general corrosion rate over time. (P_T : 3 bars, p_{CO_2} : 2 bars, free HAC: 1,000 ppm, T_g : 70°C, V_g : 5 m/s, V_l < 0.05 m/s).

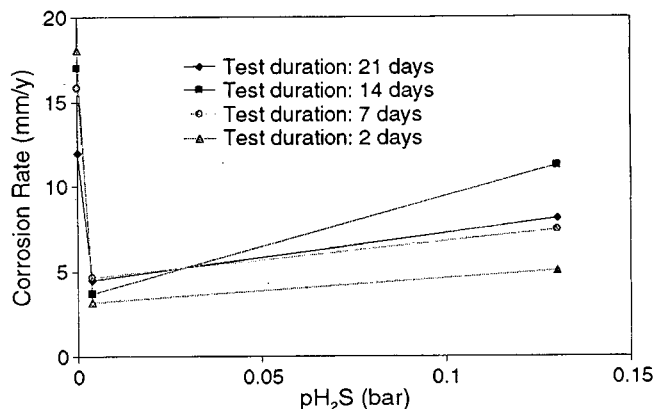


FIGURE 12. Combination of the partial pressure of H₂S and the concentration of free HAC. Evolution of the general corrosion rate with the partial pressure of H₂S. (P_T : 3 bars, p_{CO_2} : 2 bars, free HAC: 1,000 ppm, T_g : 70°C, V_g : 5 m/s, V_l < 0.05 m/s).

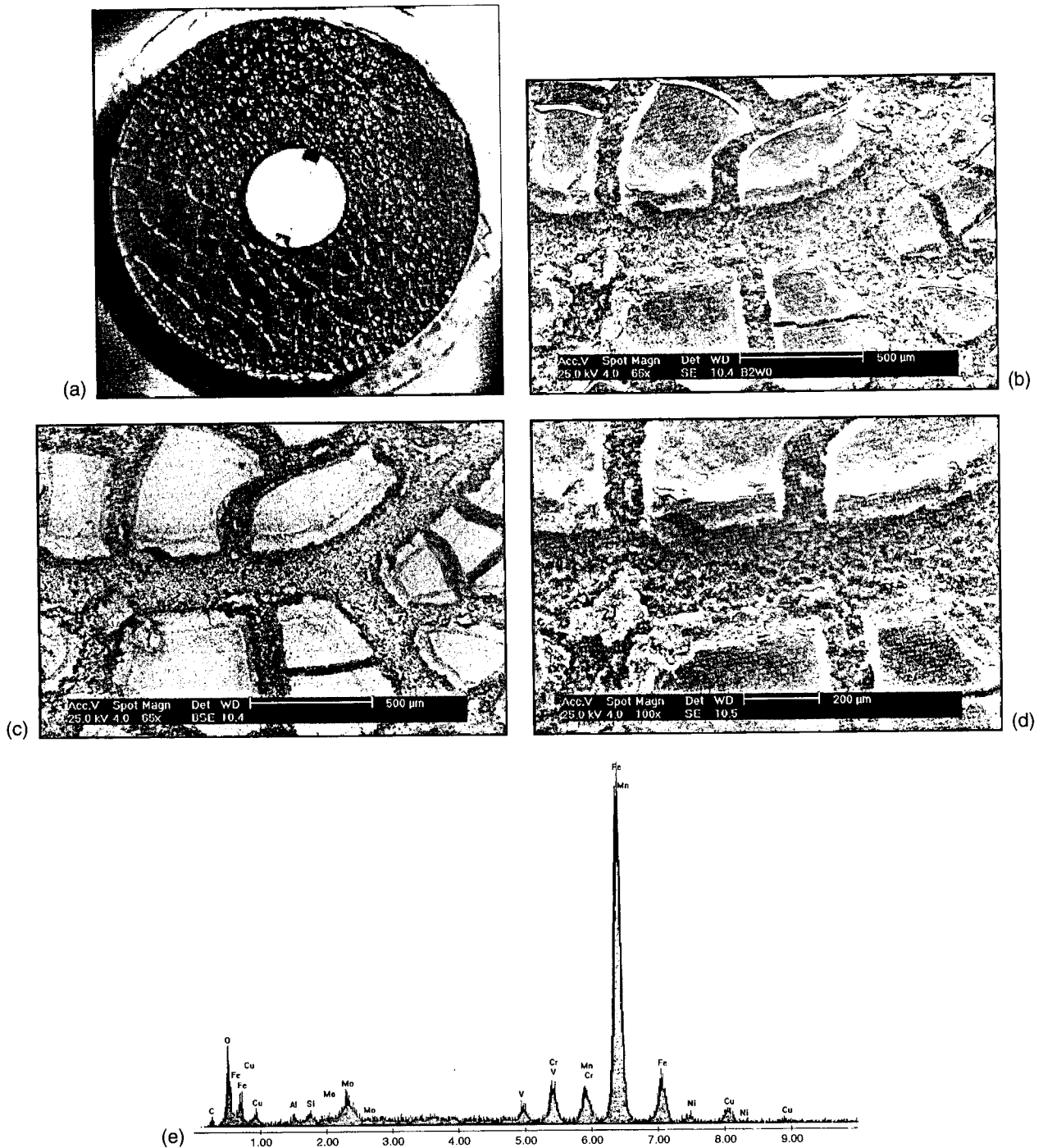


FIGURE 13. Test 1—Pure CO_2 environment: (a) WL coupon after 14 days of exposure, (b) corrosion product layer X100, (c) corrosion layer X100 back scatter, (d) corrosion product layer X200, and (e) EDS analysis of the corrosion layer. (P_r : 3 bars, $p\text{CO}_2$: 2 bars, $p\text{H}_2\text{S}$: 0 bar, free HAC: 1,000 ppm, T_g : 70°C, V_g : 5 m/s, V_l : < 0.05 m/s).

the presence of small amounts of FeCO_3 cannot be ruled out at this stage. Fe_3C forms a nonprotective, very porous film, and has been reported in some case to enhance the corrosion process by galvanic coupling (Fe_3C is electronically conductive).³⁸⁻³⁹ The numerous cracks observed in the SEM pictures of Figure 13 appeared during the dehydration process of the

weight-loss coupons; they were flushed with isopropanol immediately after their removal from the loop. There was no indication of localized corrosion and the corrosion process was strictly uniform. There was no specific influence of the nature of the corrosion product layer once acetic acid was added. However, since the corrosion rate increased with the addition of ace-

tic acid, the weight of the layer increased as well (Figure 14).

Influence of the Partial Pressure of Hydrogen Sulfide — Once traces of H_2S were added to the system, the corrosion product layer seemed fairly different. With a partial pressure of H_2S of 0.004 bar, the weight-loss coupons were covered with a very thin, visually amorphous layer (Figure 15). Even if different film structures could be observed on the surface, EDS analysis shows a similar composition. Once again, it is worth stressing that EDS is insufficient to discriminate between different types of iron sulfides, most of which have a similar elemental composition. As the partial pressure of H_2S increased, the corrosion became more severe and the corrosion product layer became thicker. The film was poorly adherent to the surface and large parts actually fell off when the coupons were processed after the tests. Even if EDS analysis gives a similar FeS film composition, the structure of the film looks different when compared to the amorphous FeS coinciding with hexagonal-shaped crystals (Figure 16). Without XRD analysis, it is difficult to characterize the film composition, but pyrrhotite or cubic FeS could form in these conditions and could match the hexagonal shape of the crystals observed.³⁰ The weight of the film increased by a factor of 100, when comparing 0.004 bar and 0.13 bar of H_2S corrosion coupons, while the corrosion rate itself only increased by a factor of 10. In the presence of 0.13 bar of H_2S , the liquid phase is strongly supersaturated with FeS . Precipitation of FeS and the direct surface reaction to form mackinawite are expected to occur simultaneously. Internal stresses are probably caused by the growth of the corrosion product film underneath the already existing layer (instead of on top of the existing layer seen in precipitation). Therefore, the growth of the scale associated with the direct surface reaction should be at the origin of the scale breakdown observed with SEM. Large parts of the coupons where the scale peeled off are much more corroded than the rest. This seems initially counter-intuitive because conventional wisdom suggests that locations with more mackinawite scale should be better protected against corrosion; however, once interpreted in the light of the argument presented above, one can accept that locations with more corrosion have seen more mackinawite formation.

Combined Effect of Acetic Acid and Hydrogen Sulfide — Figures 17 and 18 present the SEM pictures of the corrosion scale from 1,000 ppm of free acetic acid and 0.004 bar or 0.13 bar of H_2S . The FeS layer looks very similar in both cases: a uniform film, entirely cracked, thick, and non-adherent. The weight of the film is, in both cases, around 6 times what it was in the absence of any acetic acid (Figure 14). The composition of the scale is expected to be mainly mackinawite, but some crystals could be seen at 0.13 bars of H_2S (Figure 18(f)). Once again, it could be evidence

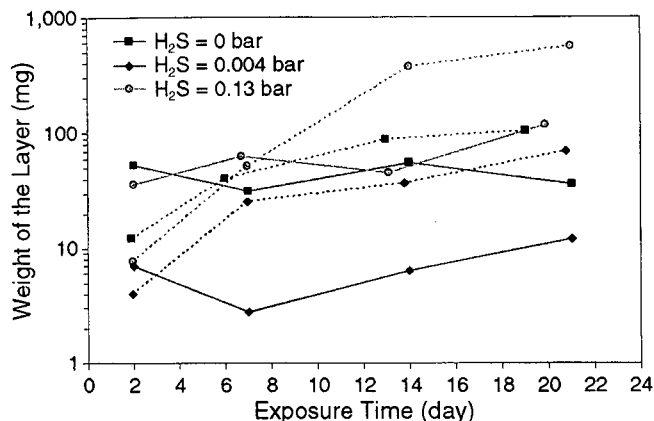


FIGURE 14. Influence of the acetic acid on the weight of the corrosion product layer. The full lines represent tests performed without free acetic acid. The dotted lines represent tests performed with 1,000 ppm of free acetic acid (P_T : 3 bars, pCO_2 : 2 bars, T_g : 70°C, V_g : 5 m/s, V_l : < 0.05 m/s).

of the presence of pyrrhotite at the higher H_2S partial pressure. Pitting corrosion is observed in Figure 17(b) and Figure 18(b) when 1,000 ppm of free acetic acid is present in the solution. The surface profile analysis presented in Figure 19 shows relatively low magnitude pitting corrosion, adding between 1 mm/y and 2 mm/y to the already high average corrosion rate (4 mm/y for test 8 and 8 mm/y for test 9).

CONCLUSIONS

- ❖ In the presence of 2 bars of CO_2 , the average corrosion at the bottom of the line (nonfilm-forming conditions) is approximately doubled when 1,000 ppm of undissociated acetic acid is present. The film present on the metal surface (most likely formed of a mixture of Fe_3C and $FeCO_3$) is unprotective and no localized corrosion could be observed.
- ❖ The presence of trace amounts of H_2S (0.004 bar) in the CO_2 environment sharply decreases the corrosion rate by two orders of magnitude. A FeS film, protective at low H_2S partial pressure, covers the surface.
- ❖ As the partial pressure of H_2S is increased to 0.13 bar, the tendency is reversed and the general corrosion rate is increased by an order of magnitude, although it never reached the high rates observed in a pure CO_2 environment. At higher H_2S content, the scale seems to break easily as a result of internal stresses and the steel not being evenly corroded.
- ❖ The introduction of 1,000 ppm of free acetic acid in the H_2S/CO_2 mixture negated the positive effects of partial pressure of hydrogen sulfide (pH_2S) and led to average corrosion rates comparable to their pure sweet condition equivalents (same order of magnitude). Some pitting and localized corrosion could be observed on the metal surface in the presence of acetic acid.

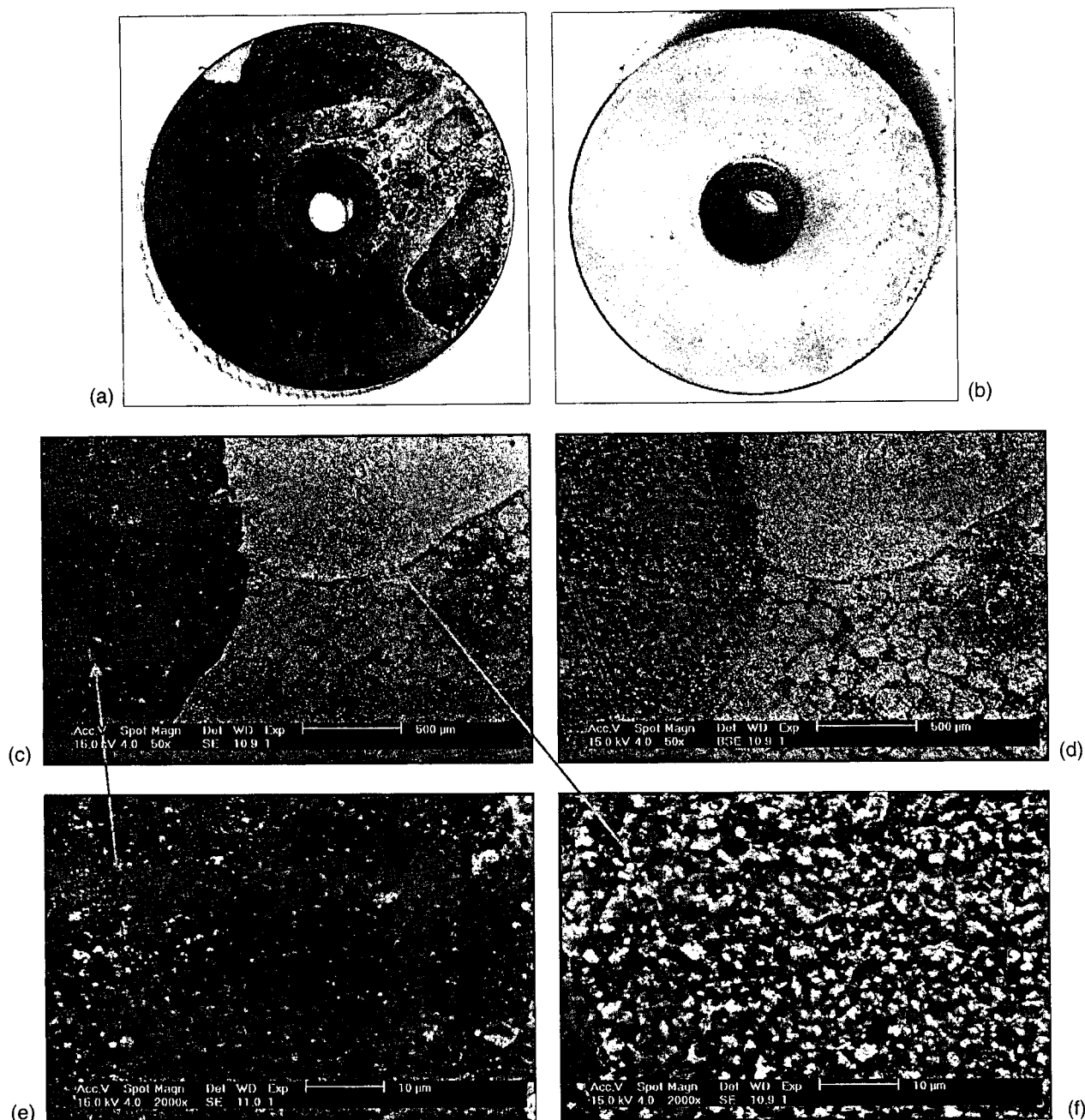


FIGURE 15. Test 4—CO₂ environment with traces of H₂S—CO₂/H₂S: 500: (a) WL coupon after 21 days of exposure, (b) WL coupon after removal of the layer, (c) corrosion product layer X100, (d) corrosion layer X50 back scatter, (e) corrosion product layer X2,000, and (f) corrosion product layer X2,000. (P_T : 3 bars, pCO_2 : 2 bars, pH_2S : 0.004 bar, free HAC: 0 ppm, T_g : 70°C, V_g : 5 m/s, V_l < 0.05 m/s).

REFERENCES

1. K. George, S. Wang, S. Nešić, C. de Waard, "Modeling of CO₂ Corrosion of Mild Steel at High Pressures of CO₂ and in the Presence of Acetic Acid," CORROSION/2004, paper no. 04623 (Houston, TX: NACE International, 2004).
2. C. De Waard, U. Lotz, "Prediction of CO₂ Corrosion of Carbon Steel," CORROSION/1983, paper no. 69 (Houston, TX: NACE, 1993).
3. B. Hedges, L. McVeigh, "The Role of Acetate in CO₂ Corrosion: The Double Whammy," CORROSION/1999, paper no. 21 (Houston TX: NACE, 1999).
4. Y. Garsany, D. Pletcher, B. Hedges, "The Role of Acetate in CO₂ Corrosion of Carbon Steel: Has the Chemistry Been Forgotten?," CORROSION/2002, paper no. 02273, (Houston, TX: NACE, 2002).
5. Y. Sun, K. George, S. Nešić, "The Effect of Cl⁻ and Acetic Acid on Localized CO₂ Corrosion in Wet Gas Flow," CORROSION/2003, paper no. 03327 (Houston, TX: NACE, 2003).
6. K. George, S. Nešić, C. de Ward, "Electrochemical Investigation and Modeling of Carbon Dioxide Corrosion on Carbon Steel in the Presence of Acetic Acid," CORROSION/2004, paper no. 04379 (Houston, TX: NACE, 2004).
7. S. Nešić, J. Postlethwaite, S. Olsen, *Corrosion* 52, 4 (1996): p. 280, doi:10.5006/1.3293640.

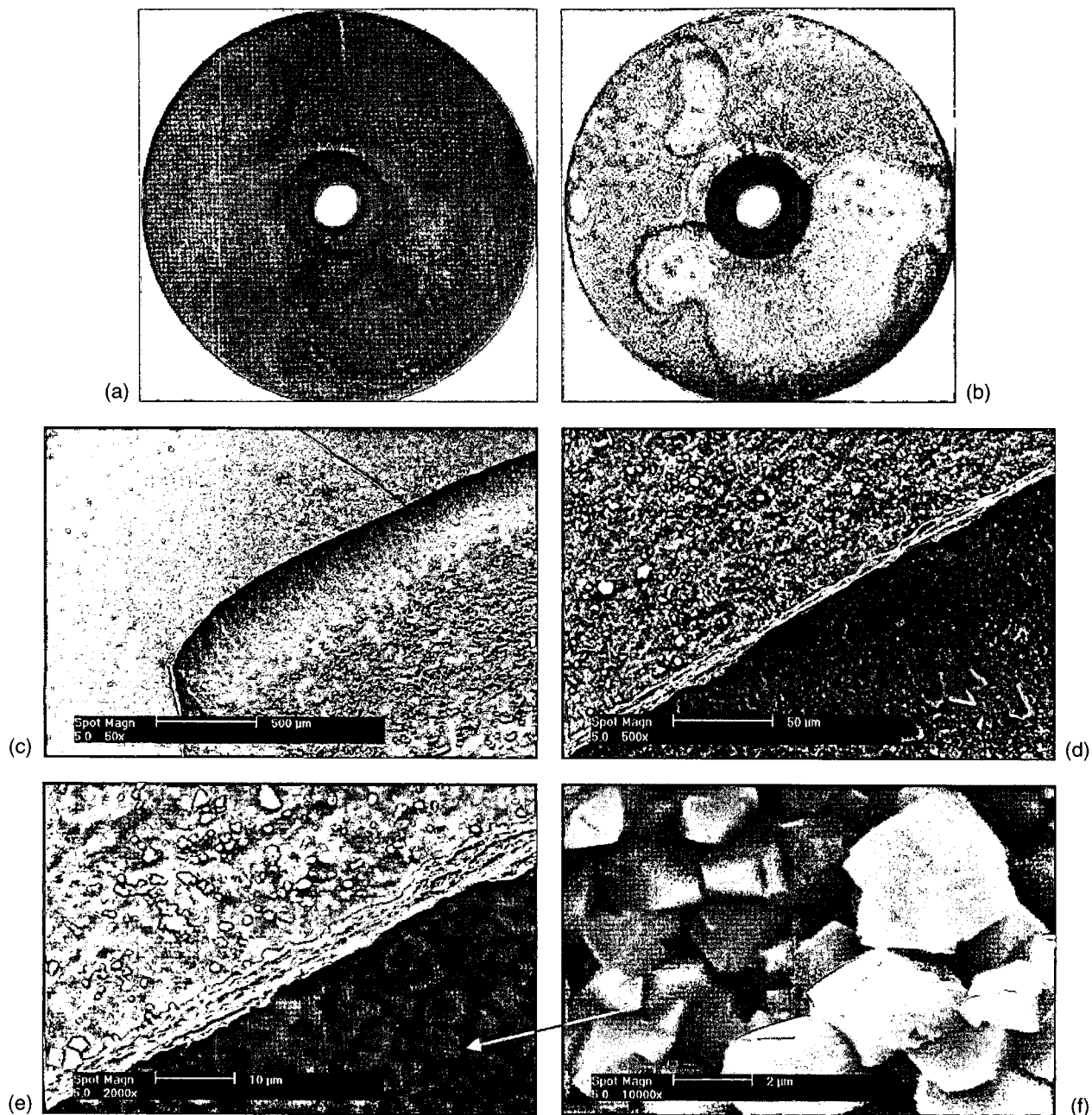


FIGURE 16. Test 6—CO₂ environment with H₂S—CO₂/H₂S: 15: (a) WL coupon after 21 days of exposure, (b) WL coupon after removal of the layer, (c) corrosion product layer X50, (d) corrosion layer X500 back scatter, (e) corrosion product layer X2,000, and (f) corrosion product layer X10,000. (P_T : 3 bars, pCO_2 : 2 bars, pH_2S : 0.13 bar, free HAc: 0 ppm, T_g : 70°C, V_g : 5 m/s, V_l < 0.05 m/s).

8. M. Nordsveen, S. Nešić, R. Nyborg, A. Stangeland, *Corrosion* 59, 5 (2003): p. 443, doi:10.5006/1.3277576.
9. J.L. Crolet, N. Thevenot, A. Dugstad, "Role of Free Acetic Acid on the CO₂ Corrosion of Steel," CORROSION/1999, paper no. 24 (Houston, TX: NACE, 1999).
10. A. Dugstad, "The Importance of FeCO₃ Supersaturation on the CO₂ Corrosion of Carbon Steel," CORROSION/1992, paper no. 14 (Houston, TX: NACE, 1992).
11. S. Nešić, K.L. Lee, *Corrosion* 59, 7 (2003): p. 616, doi:10.5006/1.3277592.
12. O. Nafday, S. Nešić, "Iron Carbonate Film Scale Formation and CO₂ Corrosion in the Presence of Acetic Acid," CORROSION/2005, paper no. 05295 (Houston, TX: NACE, 2005).
13. W. Sun, "Kinetics of Iron Carbonate and Iron Sulfide Scale Formation in CO₂/H₂S Corrosion" (Ph.D. diss., Ohio University, Chemical and Biomolecular Engineering Department, 2006).
14. J. Greenberg, M. Tomson, *Appl. Geochem.* 7 (1992): p. 185-190.
15. C.A.R. Silva, X. Liu, F.J. Millero, *J. Solution Chem.* 31 (2002): p. 97-108.
16. M. Bonis, M. Girgis, K. Goerz, R. MacDonald, "Weight-Loss Corrosion with H₂S: Using Past Operations for Designing Future Facilities," CORROSION/2006, paper no. 6122 (Houston, TX: NACE, 2006).
17. S. Smith, M. Joosten, "Corrosion of Carbon Steel by H₂S in CO₂-Containing Environments," CORROSION/2006, paper no. 06115 (Houston, TX: NACE, 2006).

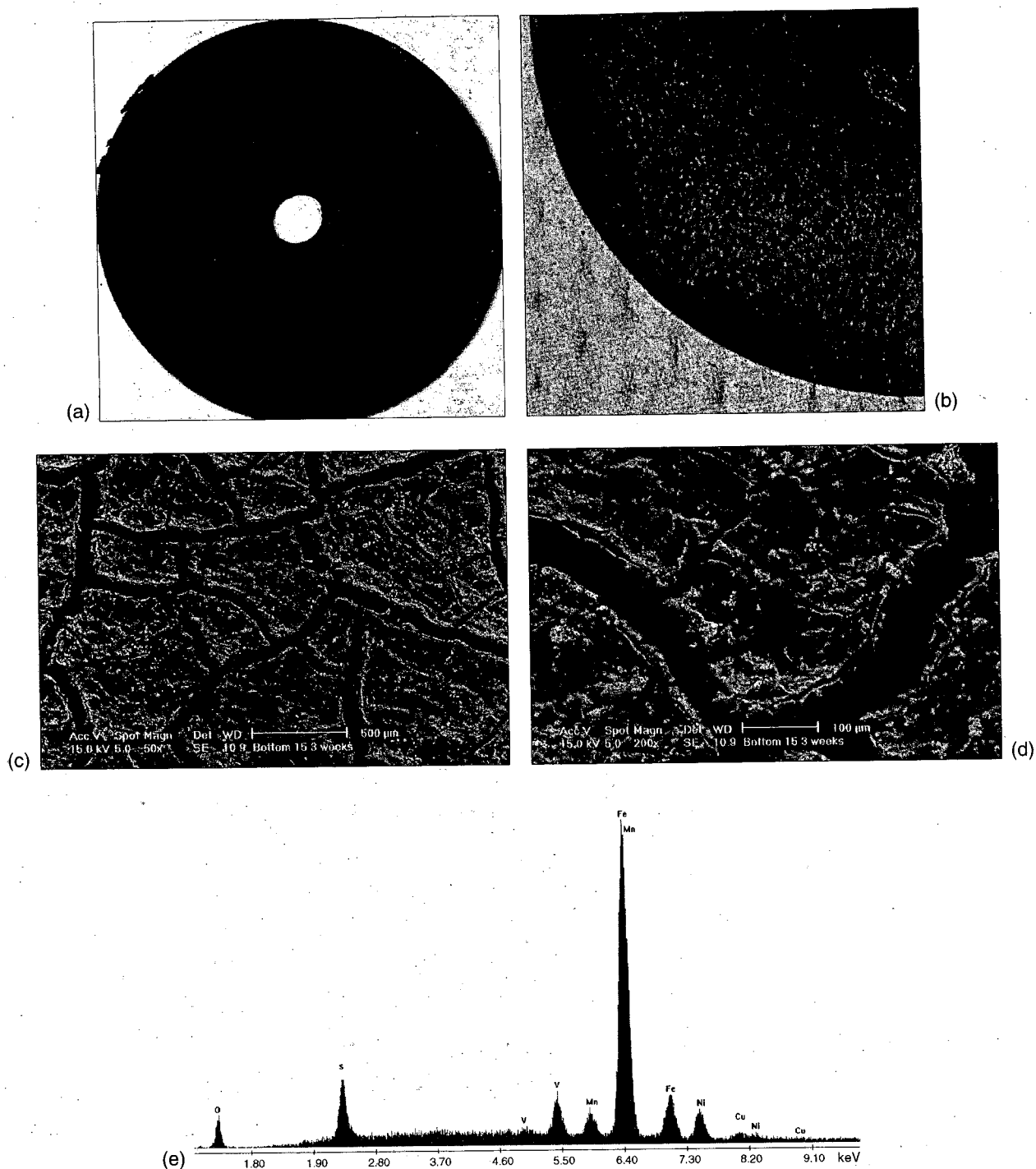


FIGURE 17. Test 7—CO₂ environment with traces of H₂S and acetic acid—CO₂/H₂S: 500: (a) WL coupon after 21 days of exposure, (b) WL coupon after removal of the layer, (c) corrosion product layer X50, (d) corrosion layer X200, and (e) EDS analysis. (P_T : 3 bars, p_{CO_2} : 2 bars, p_{H_2S} : 0.004 bar, free HAC: 1,000 ppm, T_g : 70°C, V_g : 5 m/s, V_l < 0.05 m/s).

18. W. Sun, S. Nešić, D. Young, R. Woollam, *Ind. Eng. Chem. Res.* 47 (2008): p. 1738-1742.
19. D. Rickard, G.W. Luther, *Chem. Rev.* 107 (2007): p. 514-562.
20. J. Vera, S. Kapusta, N. Hackerman, *J. Electrochem. Soc.* (1986): p. 133-461.
21. O.M. Suleimenov, R.E. Krupp, *Geochim. Cosmochim. Acta* 58 (1994): p. 2433-2444.
22. O.M. Suleimenov, T.M. Seward, *Geochim. Cosmochim. Acta* 61 (1997): p. 5187-5198.

23. L.G. Benning, R.T. Wilkin, H.L. Barnes, *Chem. Geol.* 167 (2000): p. 25-51.
24. A. Valdes, R. Case, M. Ramirez, A. Ruiz, "The Effect of Small Amounts of H₂S on CO₂ Corrosion of Carbon Steel," CORROSION/1998, paper no. 22 (Houston, TX: NACE, 1998).
25. J. Kvarekval, "The Influence of Small Amounts of H₂S on CO₂ Corrosion of Iron and Carbon Steel," Eurocorr 97 (London, U.K.: IOM Communications for European Federation of Corrosion, 1999).

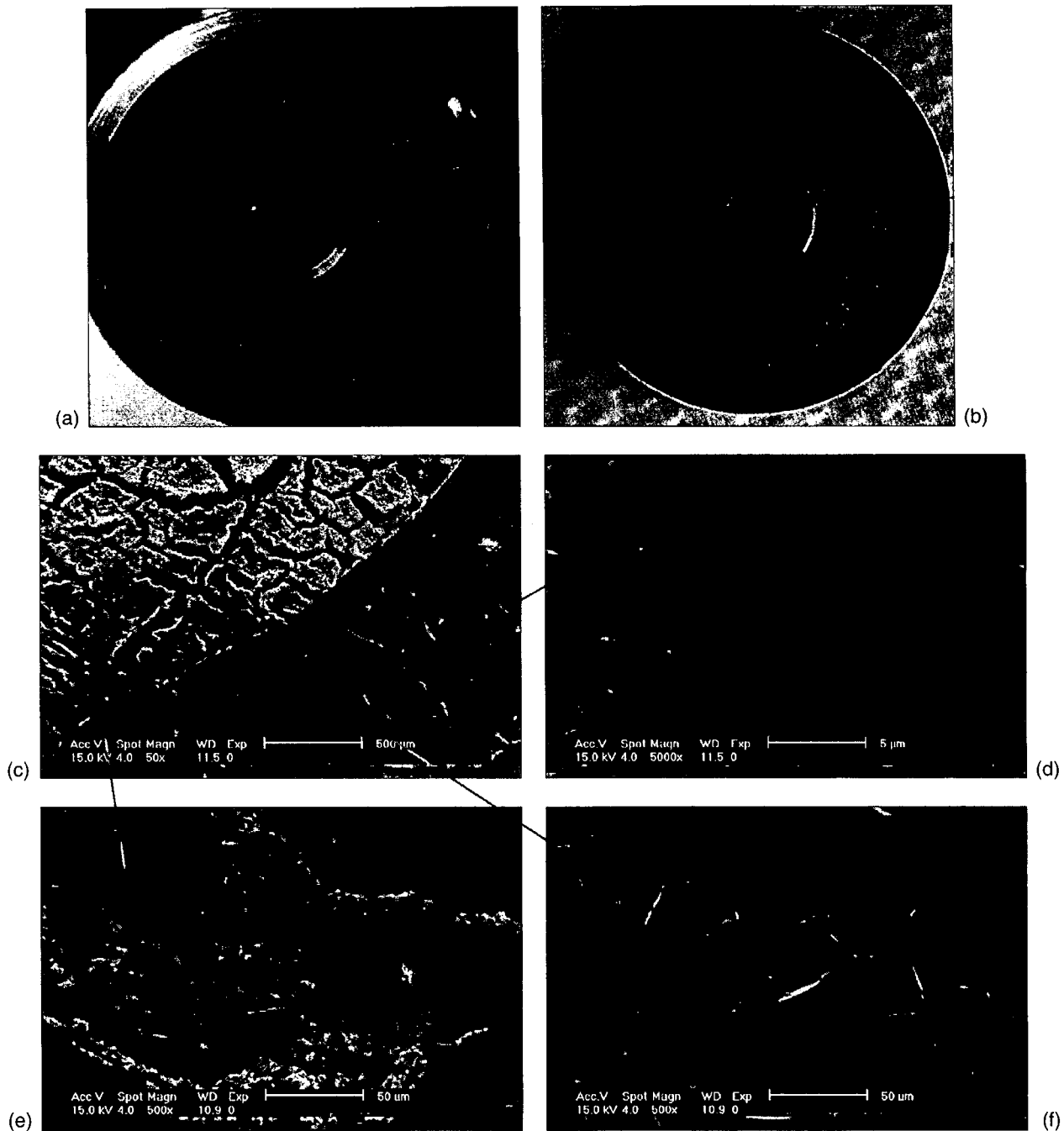


FIGURE 18. Test 9—CO₂ environment with H₂S and acetic acid—CO₂/H₂S: 15: (a) WL coupon after 21 days of exposure, (b) WL coupon after removal of the layer, (c) corrosion product layer X50, (d) corrosion layer X5,000, (e) corrosion product layer X500, and (f) corrosion product layer X500. (P_T : 3 bars, p_{CO_2} : 2 bars, p_{H_2S} : 0.13 bar, free HAC: 1,000 ppm, T_g : 70°C, V_g : 5 m/s, V_l : < 0.05 m/s).

26. B. Brown, K.L. Lee, S. Nešić, "Corrosion in Multiphase Flow Containing Small Amounts of H₂S," CORROSION/2003, paper no. 03341 (Houston, TX: NACE, 2003).
27. B. Brown, S. Reddy Parakala, S. Nešić, "CO₂ Corrosion in Presence of Trace Amounts of H₂S," CORROSION/2003, paper no. 04736 (Houston, TX: NACE, 2004).
28. W. Sun, S. Nešić, *Corrosion* 65, 5 (2009): p. 291, doi:10.5006/1.3319134.
29. B.F.M. Pots, S.D. Kapusta, R.C. John, M.J.J. Simon Thomas, I.J. Rippon, T.S. Whitham, M. Girgis, "Improvements on de Waard Milliams Corrosion Prediction and Applications to Corrosion Management," CORROSION/2002, paper no. 02235 (Houston, TX: NACE, 2002).
30. S. Smith, J.L. Pacheco, "Prediction of Corrosion in Slightly Sour Environments," CORROSION/2002, paper no. 02241 (Houston, TX: NACE, 2002).
31. A. Camacho, "CO₂ Top-of-the-Line Corrosion in Presence of H₂S" (Master's thesis, Ohio University, Chemical and Biomolecular Engineering Department, 2006).
32. M. Singer, S. Nešić, Y. Gunaltun, "Top-of-the-Line Corrosion in Presence of Acetic Acid and Carbon Dioxide," CORROSION/2004, paper no. 04377 (Houston, TX: NACE, 2004).

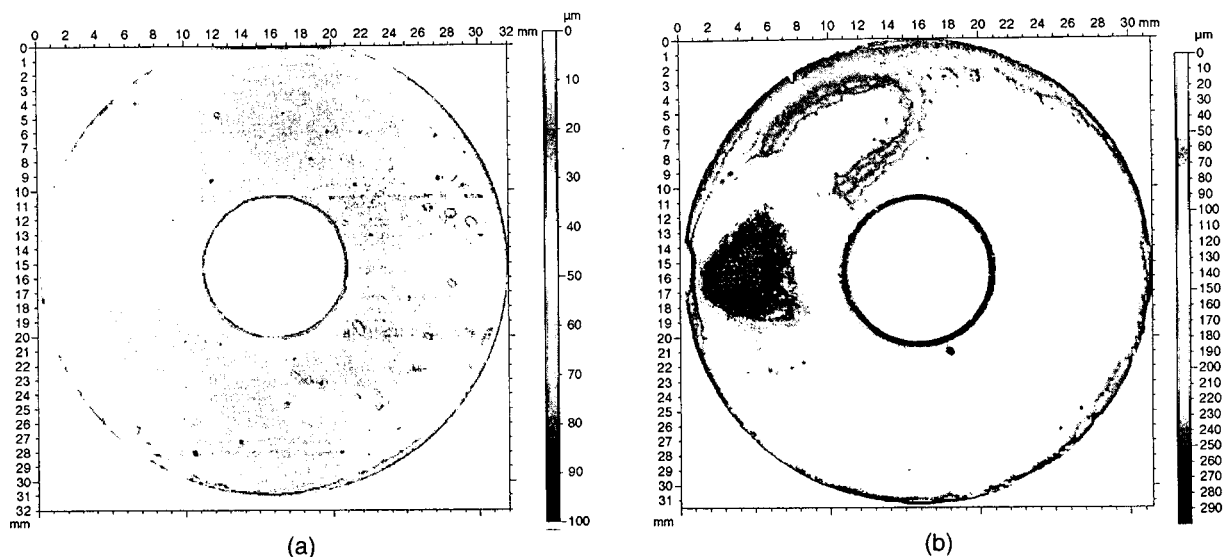
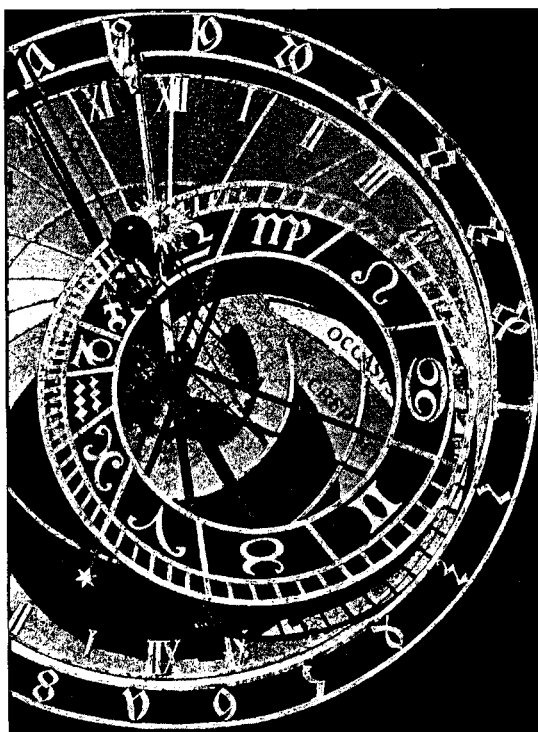


FIGURE 19. Tests 8 and 9—Localized corrosion with H_2S and acetic acid— CO_2/H_2S : 15. Surface analysis performed on weight-loss coupons after removal of the corrosion product layer: (a) Test 8— p_{H_2S} : 0.004 bar, free HAc: 1,000 ppm; WL coupon after 21 days of exposure and (b) Test 9— p_{H_2S} : 0.13 bar, free HAc: 1,000 ppm; WL coupon after removal of the layer. (P_T : 3 bars, p_{CO_2} : 2 bars, free HAc: 1,000 ppm, T_g : 70°C, V_g : 5 m/s, V_l < 0.05 m/s).

33. C. Mendez, M. Singer, A. Camacho, S. Hernandez, S. Nešić, "Effect of Acetic Acid, pH, and MEG on the CO_2 Top-of-the-Line Corrosion," CORROSION/2005, paper no. 05278 (Houston, TX: NACE, 2005).
34. S. Wang, "Effect of Oxygen on CO_2 Corrosion of Mild Steel" (Master's thesis, Ohio University, Chemical and Biomolecular Engineering Department, 2009).
35. Y.K. Kharaka, E.H. Perkins, W.D. Gunter, J.D. Debral, C.H. Bamford, "Solmineq 88: A Computer Program for Geochemical Modeling of Water Rock Interactions" (Menlo Park, CA: Alberta Research Council, 1989).
36. ASTM G1-03, "Standard Practice for Preparing, Cleaning, and Evaluating Corrosion Test Specimens" (West Conshohocken, PA: ASTM International, 2004), doi: 10.1520/G0001-03.
37. B. Craig, *Practical Oilfield Metallurgy and Corrosion*, 2nd ed. Metcorr (Tulsa, OK: PennWell Books, 1993), p. 14.
38. J.L. Crolet, S. Olsen, W. Wilhelmsen, "Influence of a Layer of Undissolved Cementite on the Rate of the CO_2 Corrosion of Carbon Steel," CORROSION/1994, paper no. 4 (Houston TX, NACE, 1994).
39. J.L. Crolet, N. Thevenot, S. Nešić, *Corrosion* 54, 3 (1998): p. 194, doi:10.5006/1.3284844.



Find more time to do what matters!

COR•Lit and MP•Lit—your source for corrosion-related abstracts.

Save research time with searchable indexes of articles appearing in *CORROSION* (COR•Lit) and *Materials Performance* (MP•Lit).

Updated annually and including more than 8,000 articles, COR•Lit provides citations of indexed articles since 1945. MP•Lit references all articles indexed since 1964.

Search by keyword or phrase to generate a list of citations identifying the issue date, article title, authors, and page number.

www.nace.org/CORLit
www.nace.org/MPLit


NACE
 INTERNATIONAL
 THE CORROSION SOCIETY